American Journal of Sciences and Engineering Research

E-ISSN– 2348–703X, Volume 8, Issue 5, 2025

Enhanced Adsorption of Rhodamine B by Iodine-Doped Bi_2MoO_6 Through Structural and Surface Modification

Mahmud Jan Mahali[1], Abdul Halim Rahmani[2], Abdul Jamil Haidari[3*]

[1,] *Chemistry Department, Faculty of Education, Jawzjan University*

[2,] *Inorganic Substances Industrial Engineering Department, Faculty of Chemical Industrial Engineering, Jawzjan University*

[3,] *Inorganic Substances Industrial Engineering Department, Faculty of Chemical Industrial Engineering, Jawzjan University*

Abstract: *Industrial dye-contaminated wastewater, predominantly originating from textile and related industries, poses a significant threat to ecosystems and human health. Rhodamine B (RhB), a water-soluble xanthene-based dye, is particularly concerning due to its potential carcinogenicity and environmental persistence. In this study, Bi_2MoO_6 (BMO), a layered Aurivillius phase oxide, was structurally and surface-modified via iodine doping to enhance its adsorption capacity for RhB. Comprehensive characterization using FTIR, XRD, XPS, SEM, and BET analyses confirmed successful incorporation of iodine, formation of BiOI phases, and substantial morphological evolution from dense nanospheres to nanoflower-like architectures with thinner nanosheets. BET measurements revealed an increased specific surface area (68.6 m^2/g for 2% I-doped BMO vs. 41.9 m^2/g for pristine BMO), indicative of an enhanced density of surface-active sites. Adsorption experiments demonstrated that 2% I-doped BMO exhibited a nearly tenfold increase in RhB uptake compared to the undoped material. Kinetic and isotherm modeling indicated pseudo-second-order kinetics and monolayer Langmuir-type adsorption behavior, with a maximum capacity of 68.83 mg/g at 25 °C and pH 4.8. These findings highlight the pivotal role of structural and surface modifications in optimizing BMO-based adsorbents for efficient dye removal from aqueous systems.*

Key words: *Bi_2MoO_6, adsorption, Rhodamine B, iodine doping, surface modification, kinetic modeling*

I. Introduction

The growth of population and industrialization has significantly impacted water pollution, making it increasingly challenging to manage [1-2]. Over the past decade, synthetic dyes have become crucial in fabric production, coatings, and pigments, with a competitive market offering various types [1-2]. The substantial discharge of toxic organic dyes by industries such as printing, textiles, leather, and papermaking poses serious threats to human health and the environment [3]. Rhodamine B (RhB), a widely used organic dye in the industry, is particularly problematic due to its high photothermal stability, making it difficult to degrade and control [4-6]. Developing effective techniques for dye removal from polluted water is crucial. Methods such as adsorption, photocatalysis, and chemical treatments are employed [7-13]. Adsorption, in particular, is recognized as a low-cost and rapid method for effectively removing organic dyes, gaining widespread use in water treatment over the past decade. A key challenge is identifying adsorbents with high performance and good reusability [14-16]. Beyond dyes, the release of untreated wastewater containing other pollutants, like antibiotics used in medicines and chemical therapies, also causes significant environmental pollution [17-20]. Wastewater often contains organic pollutants such as acid red, methylene blue, or RhB from printing industries. While various techniques

 Received-18-08-2025 Accepted- 03-09-2025

have been explored to degrade organic pollutants, many face limitations for industrial application. Consequently, adsorption methods for dye removal have attracted significant attention. Among the materials investigated, Bi-based semiconductors (e.g., Bi2WO6, Bi2MoO6, BiVO4, Bi2O2CO3, BiOX) have shown extensive study and high adsorption activity, particularly for RhB [21]. There are many methods for removal of pollutants from the environment waters, these can be classified as biological and physical purification (figure 1) gives a detailed explanation.

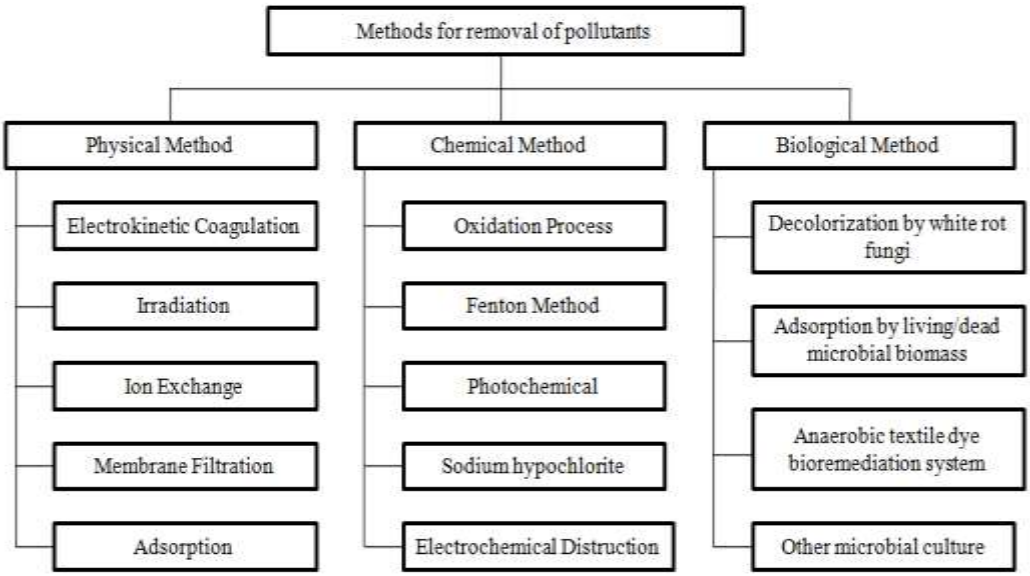

Figure 1 Methods generally in use for removal of pollutants [22].

Adsorption is a highly favored technique for removing dyes from wastewater due to its economic viability, operational flexibility, and the absence of harmful byproduct generation, contrasting with some chemical treatments that can produce foul odors or expensive waste [22-29]. Biological methods, while effective for some pollutants, can be time-consuming; for instance, mixed bacteria decolorization may require 20-30 hours [41]. Physical methods like ion exchange might be ineffective for certain dyes, and processes such as electrokinetic coagulation can generate significant sludge volumes. Adsorption, however, offers a relatively rapid, efficient, and straightforward approach for eliminating a wide range of contaminants, including dyes and heavy metals [22-29, 45]. The concept of adsorption is ancient, with the Egyptians reportedly using charcoal around 1550 BC to adsorb odorous vapors from wounds and intestines [30]. The scientific understanding of adsorption advanced significantly in the 20th century with the development of isotherm models by Freundlich and Langmuir [31]. The invention of electron microscopy in 1935 further enabled detailed characterization and quality control of adsorbent materials [32-33]. The effectiveness of an adsorption process heavily depends on the characteristics of the adsorbent used. Key properties influencing contaminant removal include specific surface area, overall surface area, pore volume, pore size distribution, and particle/grain size [34]. These parameters directly impact the adsorbent's capacity and the efficiency of the removal process. Various types of adsorbents have been investigated for dye removal. Zeolites, naturally occurring or synthetically produced microporous aluminosilicates with a negative charge, are common. For example, 3A zeolite has demonstrated the ability to remove up to 90% of pollutants like Rhodamine B (RhB) from wastewater [35, 46]. Alumina (Al2O3), a porous crystalline material with a surface area typically between 200-300 m^2/g, is effective for removing dispersed dyes [36]. Activated carbon, derived from sources like coconut shells, lignite, or coal, is perhaps the most well-known adsorbent. Despite its high effectiveness, its cost can be prohibitive for large-scale applications [37-38]. Natural, low-cost adsorbents derived from agricultural waste, such as mango peels, litchi pericarps, and jackfruit peels, are also being explored as economical alternatives [40]. Used adsorbents often require regeneration, achievable

through methods like electrochemical treatment, thermal treatment, chemical treatment, or ultrasonication [39].

The discharge of dye-laden effluents is a major environmental concern. Industries such as textiles, printing, leather, plastics, paper, and cosmetics are significant producers. The textile industry, in particular, is a major contributor, using approximately 100 liters of water to process 1 kg of textile material [42]. A substantial portion of dyes (ranging from 2% for basic dyes to 50% for reactive dyes) does not bind to the fabric and ends up in wastewater [42]. Globally, it's estimated that around 280,000 tons of textile dyes are released into the environment annually [42, 49]. These effluents are visually apparent due to their intense coloration, which not only impacts aesthetics but also blocks sunlight penetration, disrupting aquatic ecosystems [42, 45]. Even at low concentrations (as low as 1 mg/L), dyes pose threats to aquatic life and plant growth [42, 45]. Synthetic dyes, particularly azo dyes (the largest group of synthetic colorants), are problematic due to their complex molecular structures and inherent stability against oxidation, light, and biodegradation [42, 43, 47, 49]. This stability makes them resistant to conventional degradation methods. Many dyes, or their degradation byproducts, exhibit toxic, mutagenic, carcinogenic, or teratogenic properties [42, 45, 47]. Aromatic amines, potential degradation products of azo dyes, are particularly concerning [42]. The presence of dyes in water bodies increases Biochemical Oxygen Demand (BOD) and Chemical Oxygen Demand (COD), further depleting oxygen levels essential for aquatic life [42, 45]. Consequently, finding cost-effective and efficient treatment methods for dye-containing wastewater is imperative to mitigate environmental pollution and health risks [44]. Numerous treatment technologies exist for dye removal, including physicochemical methods (coagulation/flocculation, chemical oxidation, precipitation, filtration, electrolysis, photodegradation, membrane filtration, ion exchange) and biological methods (using microorganisms or biomass) [42, 45]. Traditional methods like sedimentation, chemical coagulation, and aeration have limitations, such as generating toxic sludge, high energy consumption, or requiring large treatment areas [40]. Adsorption stands out among these options due to its generally lower cost, simpler design and operation, rapid kinetics, and high effectiveness, especially for treating effluents containing recalcitrant pollutants [22-29, 40, 45]. The efficiency of adsorption is largely determined by the adsorbent's ability to capture the target pollutants. While biological treatment using living biomass can be effective for certain dyes, it is not universally applicable to all dye types [41, 47]. The complexity and stability of many synthetic dyes hinder their breakdown through biological pathways. In contrast, adsorption does not rely on biological degradation and can effectively remove a broad spectrum of dye molecules based on physical and chemical interactions with the adsorbent surface. This versatility, combined with its operational advantages, makes adsorption a widely investigated and applied technique for dye wastewater treatment [22-29, 45, 46].

Research continues to explore and develop more efficient adsorption processes. The emergence of nanoscience and nanotechnology has opened new avenues, with nanomaterials offering potentially large specific surface areas and unique properties that can enhance adsorption capacity and efficiency for dyes [48]. This ongoing research aims to address the challenges posed by the vast quantity and diverse chemical nature of dyes released into the environment, estimated at around 7 x 10^5 metric tons annually worldwide [42, 49]. Given these factors, adsorption remains a crucial and actively developed technology for the sustainable treatment of dye-contaminated industrial wastewater before its safe discharge into the environment.

II. Materials and methods

1.1. Materials

All the materials, including sodium molybdate dihydrate (Na_2MoO_4-$2H_2O$), Bismuth (III) nitrate, Bi $(NO_3)_3 \cdot 5H_2O$), ethylene glycol ($C_2H_6O_2$), ethyl alcohol absolute (C_2H_5OH), Potassium iodide (KI), RhB ($C_{28}H_{31}ClN\ _2O_3$) were of analytical grade. Pure water was well used in this study.

1.2. Synthesis of Bi_2MoO_6

All selected samples were purchased from Shangdong Honrel Company limited. Preparation of Bismuth molybdenum oxide: A concentration of (0.325 mmol, 0.0786g) $Na_2MoO_4.2H_20$ was completely dissolved in a concentration of 6ml ethylene glycol, (0.65 mmol, 0.3153g) concentration of $Bi(NO_3)_3 \cdot 5H_2O$ was dissolved in a

concentration of 6 ml of ethylene glycol and was doped wisely into $Na_2MoO_4 \cdot 2H_2O$ solution, the experiment was allowed to stir for 30 minutes. A concentration of 30 ml of absolute ethanol was added, which was allowed to stir at room temperature for 2 hours; the mixture was transferred to an autoclave lined with Teflon and aged at 160 °C for 24 hours. Then the material was washed several times with distilled water and absolute ethanol and dried in the oven at 55°C for 12hours, and ground well for further use [83].

1.3. Synthesis of I-doped BMO

All selected samples for this synthesis were purchased from Shangdong Honrel Company limited. Preparation of KI: A concentration of 0.325 mmol, 0.0786g of Na2MoO4·2H2O was dissolved in 6 ml of ethylene glycol. A concentration of 0.65 mmol, 0.3153 g of Bi(NO3)3·5H2O was dissolved in 6 ml of ethylene glycol and dropped wisely into Na2MoO4·2H2O solution and allowed to stir for 30minutes. A concentration 30 ml of absolute ethanol was added with different concentration of KI was doped in the mixture, when I : Mo = 0.1, I : Mo = 0.2, I : Mo = 0.4, I : Mo = 0.6, I : Mo = 0.8, I : Mo = 1.0, I : Mo = 1.6, I : Mo = 2.0, I : Mo = 2.6, I : Mo = 3.0 were prepared respectively and stirred at room temperature for 2 hours, Then the mixture was transferred to a 50mL autoclave and reacted 160 °C for 24 hours. After naturally cooling at room temperature, Then the material was washed several times with distilled water and absolute ethanol and dried in the oven at 55 °C for 12hours, and ground well for further use.

1.4. Characterization of BMO adsorbents

The synthesized samples were examined by Fourier transform infrared spectroscopy (FTIR, Nicolet iS5) operated on a spectrometer from 4000-400 cm−1, at a resolution of 2 cm−1 with 70 scans averaging five spectra using KBr pellets (forms a translucent sheet in the infrared region and allows a 100% communication window in the range of wave number through the samples) [84]. The synthesized samples were examined by X-ray diffraction analysis which was recorded on a D8 Advance with Cu Kα as a radiation source ranging from 1-80°. The X-ray was applied to examine the morphologies of the synthesized samples [85]. The surface composition of the samples was analyzed by X-ray photoelectron spectroscopy (XPS, EscaLab Xi+, ThermoFisher, USA) with Al Ka radiation. The chemical and electronic states of the atoms within the synthesized material, as well as the elemental composition, were analyzed. The XPS spectrum is obtained by irradiating a solid surface with an X-ray beam and measuring the kinetic energy of the electrons emitted from the top 1-10 nm of the material. The photoelectron spectrum is recorded by counting the emitted electrons over a range of kinetic energy. The energy and intensity of the photoelectron peak enable the identification and quantification of all surface elements [86]. The morphology of the synthesized samples was examined by scanning electron microscopy (SEM) using a TESCAN MIRA LMS field. It was used to detect the sample section at an acceleration voltage of 15 Kv. [87].

1.5. Adsorption studies for BMO

Adsorption studies were conducted in the dark to prevent the degradation of RhB. In these experiments, 20 mg of Bi_2MoO_6 was continuously dispersed into 50 mL of RhB solution with concentrations ranging from 10 to 300 mg/L. The mixture was then vigorously stirred using a magnetic stirrer for 3 hours at room temperature and subsequently centrifuged at 10,000 rpm for 3 minutes. Finally, the collected samples were transferred into a microcell for the determination of RhB concentration at 554 nm using UV-Vi's spectrophotometry.

1.6. Adsorption studies for I-doped BMO

Adsorption studies were carried out in the dark to prevent the degradation of RhB. In these experiments, 20 mg of I-doped BMO was continuously dispersed into 50 mL of RhB solution with concentrations ranging from 10 to 300 mg/L. The resulting mixture was stirred for 3 hours using a magnetic stirrer under different temperature conditions (25 °C, 35 °C, and 45 °C), followed by centrifugation at 10,000 rpm for 3 minutes. Finally, the collected samples were transferred into a microcell for the determination of RhB concentration at 554 nm using UV-Vi's spectrophotometry [89].

III. Result and Discussion

1.7. Fourier Transform Infrared (FTIR) spectroscopy Analysis

The fourier transform infrared spectroscopy (FTIR) spectra of the synthesized samples are shown in Figure 2. The broad band at (3200-3600 cm-1) and (1500-1650 cm-1) are attributed to O-H group of the adsorbed water molecules on the surface [90]. The peaks in the range of 1000-1500 cm-1 are corresponded to C=O and C-O stretching in CO2 impurities on the surface of catalysts [91]. The peak located at 439 cm-1 is assigned to be the Bi-O vibration [92]. The two characteristic bands at 565 and 728 cm-1 are corresponded to the bending and asymmetric stretching of Mo-O in MoO6 octahedrons which could be related to the equatorial oxygen atoms [93]. The peaks at 794 and 841 cm-1 are also originated from the asymmetric and symmetric stretching modes of the apical oxygen atoms in MoO6 [94].

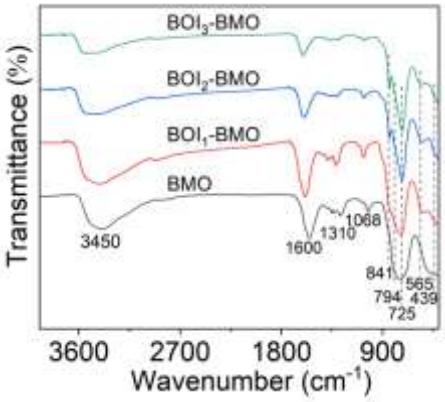

Figure 2. FTIR of BMO, BOI_1-BMO, BOI_2-BMO and BOI_3-BMO

1.8. XRD characterization

The XRD patterns for the synthesized samples were recorded and shown in Figure 3. For the pure BMO, the diffraction peaks observed at 2θ = 28.3°, 32.5°, 46.7°, 55.44°, and 58.4° were assigned to the 131, 002, 202, 331, and 262 crystal planes of orthorhombic Bi2MoO6 (JCPDS no. 76-2388). When the ratio of I : Mo = 1, no other miscellaneous peaks are found. This may be due to the low doping amount of I. When the ratio increases to 2, there is an extra peak at 31.7. When the ratio is 3, more peaks appear at 31.7°, 45.5° and 51.5°. These peaks correspond to tetragonal BiOI (JCPDS no. 73-2062) [95].

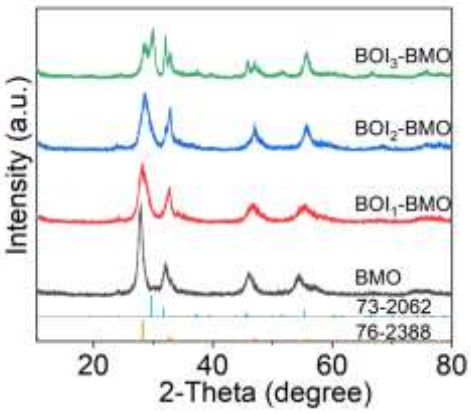

Figure 3. XRD pattern of BMO, BOI1-BMO, BOI2-BMO and BOI3-BMO

1.9. XPS analysis

Overall, XPS spectra of BMO and BOI2-BMO samples are shown in Figure 4. (a). Eight peaks corresponding to Bi 5d5, Bi 4f, Mo3d, C 1s, Bi4d5, Bi4d3, O1s, and Bi4p3 were observed for both BMO and BOI2-BMO. I4d and I3d peaks appear for BOI2-BMO. The presence of C 1s peak has been attributed to contamination by base material

for calibration. As shown in figure 4. (d) two sets of Bi 4f spin-orbit doublet components are observed, including Bi 4f5/2 and Bi 4f7/2. The Bi 4f spectra can be decomposed into four peaks at 157.9, 159.7, 162.9 and 165.0 eV for BMO and 158.7, 159.5, 164.2 and 165.0 eV for BOI2-BMO. The peaks at 157.9, 162.9, 158.7 and 164.2 eV are assigned to the Bi 3+ species and the peaks at 159.7, 165.0, 159.5 and 165.0 eV are assigned to the Bi 5+ species. Furthermore, this indicates that the I doping had no effect on the chemical state of bismuth. From figure 4. (c), the Mo 3d XPS spectrum of BMO consists of two symmetrical peaks at 231.3 and 234 eV, corresponding to Mo 3d 5/2 and Mo 3d 3/2, respectively. The Mo 3d XPS spectrum of BOI2-BMO is also composed of two symmetrical peaks at 232 and 235.5 eV, corresponding to Mo 3d 5/2 and Mo 3d 3/2, respectively. All peaks are characteristic of Mo 6+ species. The O 1s XPS spectra of BMO and BOI2-BMO samples are shown in Figure 4. (b). For O 1s XPS spectra, the asymmetric peek can be decomposed into two peak at 529.8 and 530.2 eV for BMO, 530 and 533.3 eV for BOI2-BMO, and these peeks assigned to surface lattice oxygen (Olatt) and adsorbed oxygen (Oads) species, respectively [96]. Bi/Mo molar ratio close to 2.0, Indicates that the BMO and BOI2-BMO samples are well proportioned. The surface Bi5+/Bi3+ and Oads /Olatt molar ratios increased after iodine doping, which helps to improve adsorption activity.

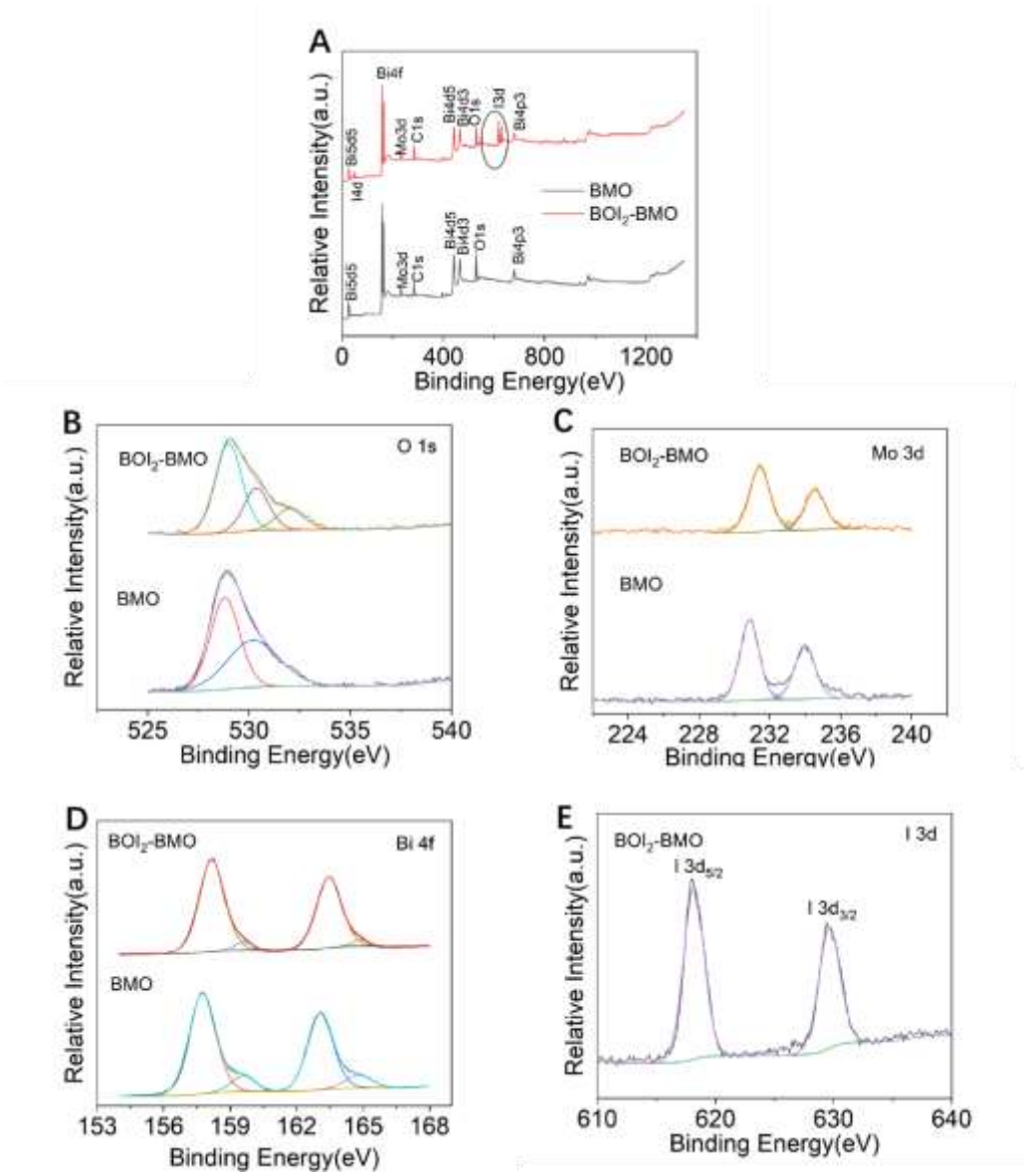

Figure 4. XPS survey scans of (a) BMO and BOI_2-BMO. High-resolution spectra of (b) O Is (c) Mo 3d (d) Bi 4f (e) I 3d.

1.10. Morphology analysis

The Scanning Electron Microscopy (SEM) of the synthesized pure BMO and I : Mo = 2.0 concentration of I-doped BMO are shown in Figure 5. The pure BMO is a self-assembled nanosphere composed of thick nanosheets (Figure 5(a-b)). When doped with I, in Figure 5(c-d) the nanosheets become thinner and the nanospheres form nanoflowers. This structure provides a large number of adsorption binding sites to transport pollutants to the surface of the adsorbent, thus improving the adsorption performance [97-98].

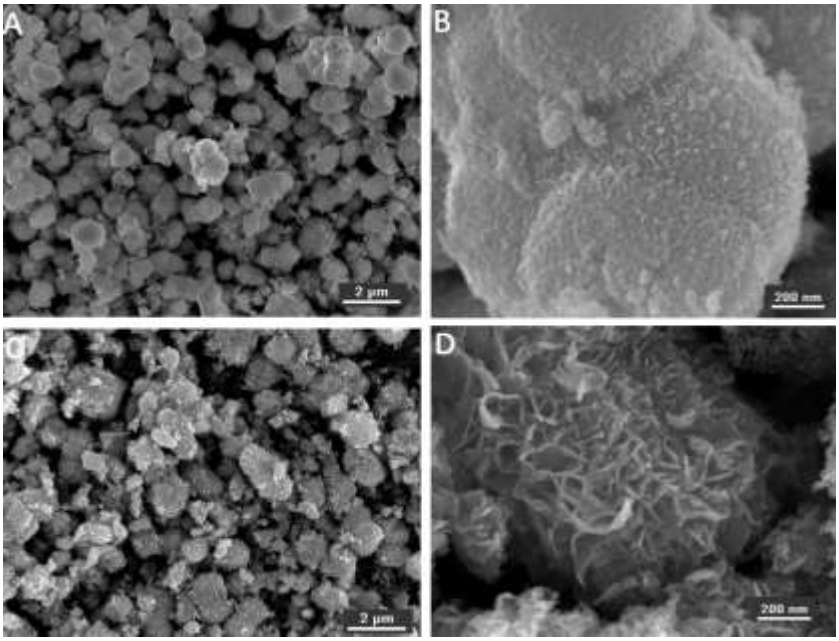

Figure 5. SEM images of (a-b) BMO and (c-d) BOI_2-BMO

1.11. Brunauer, Emmett and Teller (BET) Analysis

The Brunauer Emmett and Teller (BET) surface area of pure BMO and I-doped BMO was determined by N2 adsorption which are shown in (figure 6a. and 6b). The N2 adsorption curves was assigned as a type (IV) isotherm with a H_3 hysteresis loop, indicating a mesoporous structure. This proves that I-doped Bi_2MoO_6 has largest surface area of 68.6 m2. g-1 which is much larger that pure BMO of value 41.9 m2. g-1. which also shows that I doped BMO has high adsorption performance. The large BET surface area provides more active sites to ensure easy adsorption of RhB and also facilitates the rapid transfer of adsorbate [99].

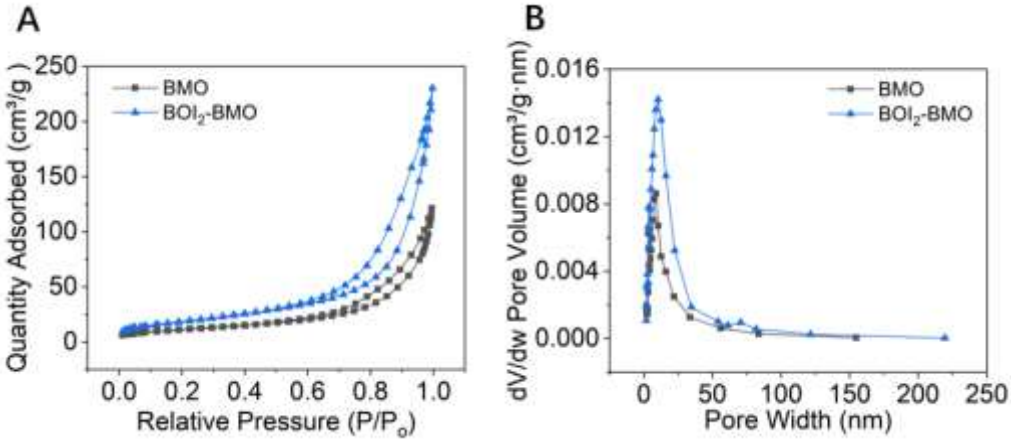

Figure 6. (a) Adsorption desorption curve and (b) pore size distribution curve of BMO and BOI2-BMO

1.12. Concentration of I-doped BMO

I-doped BMO, concentration of I : Mo = 0.1, I : Mo = 0.2, I : Mo = 0.4, I : Mo = 0.6, I : Mo = 0.8, I : Mo = 1.0, I : Mo = 1.6, I : Mo = 2.0, I : Mo = 2.6, I : Mo = 3.0 were synthesized via hydrothermal method respectively, the I-doped BMO samples exhibited much higher adsorption activity and I : Mo = 2.0 doped BMO (BOI2-BMO) shows the highest RhB adsorption rate, this was 10 times higher than pure BMO.

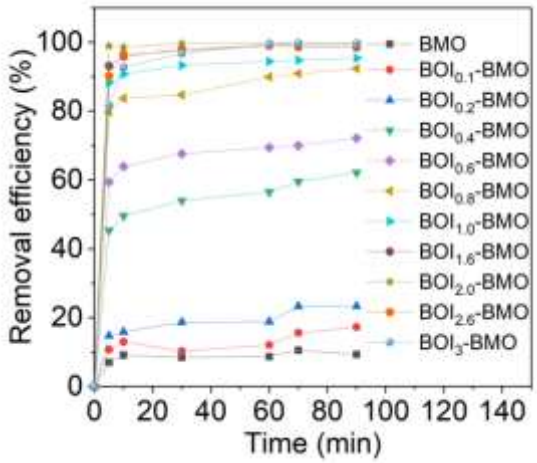

Figure7. Effect of I doping concentration on adsorption of RhB

1.13. Effect of adsorbent amount

Results from different concentration of the absorbent 10 mg, 20 mg, 30 mg, 50 mg was investigated, all the different concentrations showed good absorption capacity but at 20 mg appears to have reached almost 95% RhB adsorption, The reason in this study, 20 mg was considered the best and used in all the characterization Technique tests that was carried out on the sample.

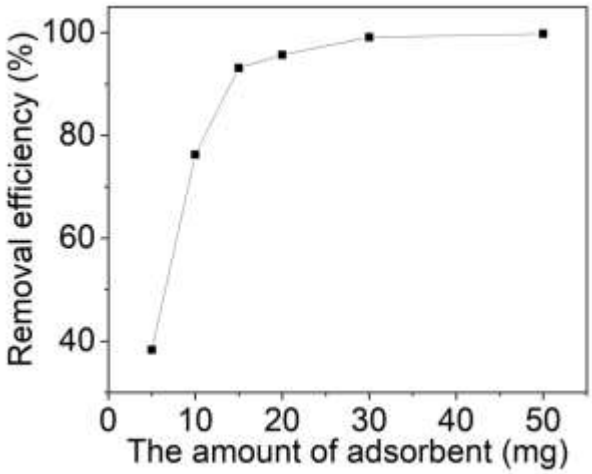

Figure 8. Effect of concentration of BOI2-BMO on adsorption of 10 mg/L RhB

1.14. Adsorption Kinetics

The dye adsorption kinetics of the synthesized I-doped BMO was carried out in RhB concentration solution of 10 mg/L. The RhB solution adsorption capacity of BOI2-BMO versus adsorption time is showed in figure (9). The kinetic data was accessed using pseudo-first-order and pseudo-second-order kinetics models aiming to further understand the mechanism of adsorption behavior, the adsorption kinetics studied by time change and concentration change shows that the adsorption data of BOI2-BMO follow the pseudo second-order kinetics [100]. The mathematical formulas of the two kinds of the models are shown below;

$$\ln (Q_e - Q_t) = \ln Q_e - k_1 t \quad (1)$$

Where Qe and Q t (mg · g-1) are the RhB adsorption amounts at equilibrium and at time. k1 is the rate constant (min-1) [101].

$$\frac{t}{Q_t} = \frac{1}{k_2 Q_e^2} + \frac{t}{Q_e} \quad (2)$$

Where k_2 is the rate constant ($g \cdot mg^{-1} \cdot min^{-1}$).

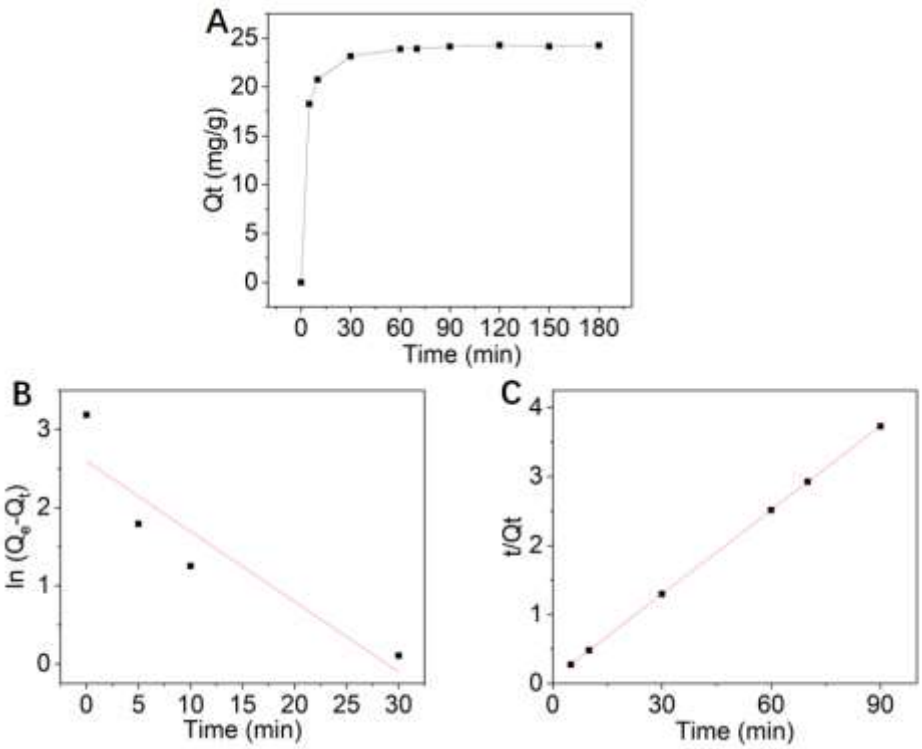

Figure 9 (a) Time-dependent adsorption behavior of 20 mg BOI_2-BMO in 10 mg/L RhB, (b) pseudo-first-order kinetics plots of ln (Q e -Q t) vs. t and (c) pseudo-second-order kinetics plots of t/Q t vs. t.

1.15. Effect of pH value

The pH value is vital in affecting the adsorption capacity of BOI2-BMO because the pH value of the solution can change the existing forms of RhB molecules, the pH is adjusted by adding hydrochloric acid (0.1N) or sodium hydroxide (0.1N), due to the competition between H+ ions and molecules of RhB to occupy the adsorption sites. In this research, the effect of pH values ranging from 2 to 10 was tested and investigated by adding a substantial amount of B-R buffer solution, as shown in Figure 11. The figure below shows the adsorption capacities of different BOI2-BMO synthesized samples at different pH values; the highest adsorption capacity of all synthesized BOI2-BMO samples was obtained when the pH value was adjusted to 2. As the pH value of the synthesized solution is increased with values ranging from (2 to 10), the adsorption capacity decreases as well. This is due to the adsorption of RhB on BOI2-BMO being attributed to electrostatic interactions. Also, whiles the pH increases, the dissociation of BOI2-BMO is inhibited accordingly, which leads to a decrease in the RhB adsorption capacity [100].

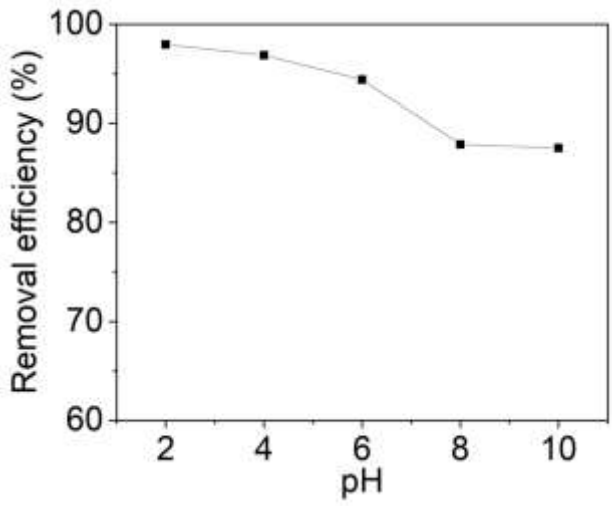

Figure 11. Adsorption capacities of BOI_2-BMO for RhB at different pH values

IV. Conclusion

The novel I-doped BMO (I:Mo=2) synthesized during this project exhibited excellent adsorption capacity for RhB that was 10 times higher than unmodified BMO. I-doped BMO was characterized by FTIR, XRD, XPS, SEM, and BET. Results indicated, that while unmodified BMO formed self-assembled nanospheres composed of thick nanosheets, I-doped BMO was shaped into nanoflowers with thinner nanosheets. As confirmed by the BET experiment, the nanoflower structure provides a larger number of surface binding sites for organic pollutants, thus improving adsorption performance. FTIR and XRD spectroscopy confirmed the succesful synthesis of unmodified BMO and I-doped BMO. FTIR showed functional groups comprised into the BMO chemical structure. XRD for unmodified BMO, the exhibited diffraction peaks at 28.3°, 32.5°, 46.7°, 55.44°, and 58.4° assigned to the 131, 002, 202, 331, and 262 crystal planes of orthorhombic BMO. When BMO was doped with large quantities of I, additional peaks appeared at 31.7°, 45.5°, and 51.5°. These peaks correspond to tetragonal BiOI. XPS survey spectra of BMO and BOI2-BMO samples had eight corresponding peaks corresponding to Bi 5d5, Bi 4f, Mo3d, C 1s, Bi 4d5, Bi 4d3, O 1s, and Bi 4p3. I 4d and I 3d peaks appeared for BOI2-BMO. The O 1s XPS high-resolution spectra of BMO and BOI2-BMO showed two asymmetric peek at 529.8 and 530.2 eV for BMO and at 530.0 and 533.3 eV for BOI2-BMO. These peaks were assigned to surface lattice oxygen (Olatt) and adsorbed oxygen (Oads) species, respectively. Interestingly, the Oads/Olatt as well as the the surface Bi5+/Bi3+ molar ratios increased after I doping, which facilitates adsorption activity. RhB adsorption by I-doped BMO was optimal at pH 2 and was consistent with the Langmuir isotherm adsorption model and the pseudo-second-order kinetics. The Langmuir isotherm adsorption model means this process belongs to monolayer adsorption. The pseudo-second-order kinetics model assumes the adsorption process largely pertains to the chemisorption that the rate limiting stage related to the electrons sharing or exchange between I-doped BMO and RhB. In summary, I-dope BMO is a low-cost and environmentally-friendly adsorbent showing great potential for practical application in the field of water treatment.

V. References

[1] Titchou F, Zazou H, Afanga H, et al. Removal of persistent organic pollutants (POPs) from water and wastewater by adsorption and electrocoagulation process[J]. Groundwater for Sustainable Development, 2021, 13: 570-575.

[2] Acharya J, Kumar U, Rafi, P, et al. Removal of heavy metal ions from wastewater by chemically modified agricultural waste material as potential adsorbent-a review. International Journal of Current Engineering and Technology, 2018, 8(3): 526-530.

[3] Dąbrowski A. Adsorption-from theory to practice[J]. Advances in Colloid and Interface Science, 2001, 93: 135-224.

[4] Langmuir I. The adsorption of gases on plane surfaces of glass, mica and platinum[J]. American Chemical Society, 1918, 409: 1361-1403.

[5] McMullan D. Scanning electron microscopy 1928–1965[J]. Scanning, 1995, 17: 175-185.

[6] Williams D, Carter B. The transmission electron microscope, in: Transmission electron microscopy[J]. Springer, 1996, 34: 3-17.

[7] Rouquerol J, Rouquerol B, Llewellyn P, et al. Adsorption by powders and porous solids: principles, methodology and applications[J]. Academic Press, 2013, 62: 72-74.

[8] Shi B, Li G, Wang D, et al. Removal of direct dyes by coagulation: The performance of preformed polymeric aluminum species[J]. Hazardous Materials, 2007, 143: 567-574.

[9] Lima B, Royer M, Bach G, et al. Comparison of Spirulina platensis microalgae and commercial activated carbon as adsorbents for the removal of Reactive Red 120 dye from aqueous effluents[J]. Hazardous Materials, 2012, 241: 146-153.

[10] Tan K B, Vakili M, Hord B A, et al. Adsorption of dyes by nanomaterials: Recent developments and adsorption mechanisms[J]. Separation and Purification Technology, 2015, 150: 229-242.

[11] Gupta V K, Suhas. Application of low-cost adsorbents for dye removal-A review[J]. Environmental Management, 2009, 90: 2313-2342.

[12] Zhao G, Liu L, Liu Q, et al. Efficient removal of dye MB: Through the combined action of adsorption and photodegradation from $NiFe_2O_4/Ag_3PO_4$[J]. Alloys and Compounds, 2016, 664: 169-174.

[13] Xu C, Wu H, Gu F L. et al. Efficient adsorption and photocatalytic degradation of Rhodamine B under visible light irradiation over BiOBr/montmorillonite composites[J]. Hazardous Materials, 2014, 275: 185-192.

[14] Wang Y, Yao M, Chen Y, et al. General synthesis of magnetic mesoporous FeNi/graphitic carbon nanocomposites and their application for dye adsorption[J]. Alloys and Compounds, 2015, 627: 7-12.

[15] Rafique M A, Jamal A, Afzal G, et al. Photocatalytic mediated remediation of synthetic dyes effluent using zero-valent iron: a comparative study[J]. Desalination and Water Treatment, 2021, 237: 284-291.

[16] Yang C, Wu S, Cheng J, et al Indium-based metal-organic framework/graphite oxide composite as an efficient adsorbent in the adsorption of rhodamine B from aqueous solution[J]. Alloys and Compounds, 2016, 687: 804-812.

[17] Ali I. New generation adsorbents for water treatment[J]. Chemical Reviews, 2012, 10: 5073-5091.

[18] Wang C, Li J, Guo G, et al. Photocatalytic organic pollutants degradation in metal–organic frameworks[J]. Energy & Environmental Science, 2014, 79: 2831–2867.

[19] Bazrafshan E, Alipour M R, Mahvi A H. Textile wastewater treatment by application of combined chemical coagulation, electrocoagulation, and adsorption processes[J]. Desalination and Water Treatment, 2016, 57: 9203-9215.

[20] Zhou S, Watanabe H, Wei C, Wang D, Zhou J, Tatarazako N, et al. Reduction in toxicity of coking wastewater to aquatic organisms by vertical tubular biological reactor[J]. Ecotoxicology and Environmental Safety, 2015, 115: 217-222.

[21] Yadav A, Mukherji S, Garg A. Removal of Chemical Oxygen Demand and Color from Simulated Textile Wastewater Using a Combination of Chemical/Physicochemical Processes[J]. Industrial and Engineering Chemistry Research, 2013, 52: 10063-10071.

[22] Fang Y, Huang Q, Liu P, et al. Easy-separative MoS_2-glue sponges with high-efficient dye adsorption and excellent reusability for convenient water treatment[J]. Colloids and Surfaces A: Physicochemical and Engineering Aspects, 2018, 540: 112–122.

[23] Iriarte-Velasco U, Chimeno-Alanis N, Gonzalez-Marcos M P, et al. Relationship between Thermodynamic Data and Adsorption/Desorption Performance of Acid and Basic Dyes onto Activated Carbons[J]. Chemical & Engineering Data, 2011, 56: 2100-2109.

[24] Acar E T, Ortaboy S, Atun G, et al. Adsorptive removal of thiazine dyes from aqueous solutions by oil shale and its oil processing residues: Characterization, equilibrium, kinetics and modeling studies[J]. Chemical Engineering Journal, 2015, 276: 340-348.

[25] Bai S, Shen X, Zhong X, et al. One-pot solvothermal preparation of magnetic reduced graphene oxide-ferrite hybrids for organic dye removal[J]. Carbon, 2012, 50: 2337-2346.

[26] Chen M, Huang Y, Chu W. et al. Exploring a broadened operating pH range for norfloxacin removal via simulated solar-light-mediated Bi_2WO_6 process[J]. Chinese Journal of Catalysis, 2019, 40: 673-680.

[27] Yu C, He H, Liu X, et al. Novel SiO_2 nanoparticle-decorated BiOCl nanosheets exhibiting high photocatalytic performances for the removal of organic pollutants[J]. Chinese Journal of Catalysis, 2019, 40: 1212-1221.

[28] Yang K, Li X, Zeng D, et al. Review on heterophase/homophase junctions for efficient photocatalysis: The case of phase transition construction[J]. Chinese Journal of Catalysis, 2019, 40: 796-818.

[29] Yu C, He H, Zhou W, et al. Novel rugby-ball-like Zn-3(PO_4) (2) @C_3N_4 photocatalyst with highly enhanced visible-light photocatalytic performance[J]. Separation and Purification Technology, 2019, 217: 137-146.

[30] Hu J, Chen D, He J, et al. Recyclable Carbon Nanofibers@Hierarchical I-Doped $Bi_2O_2CO_3$-MoS_2 Membranes for Highly Efficient Water Remediation under Visible-Light Irradiation[J]. ACS Sustainable Chemistry & Engineering, 2018, 6: 2676-2683.

[31] Rahmani M, Sasani M. Evaluation of 3A zeolite as an adsorbent for the decolorization of rhodamine B dye in contaminated waters[J]. Applied Chemistry, 2016, 41: 83-90.

[32] Hegazi H. Removal of heavy metals from wastewater using agricultural and industrial wastes as adsorbents[J]. HBRC, 2013, 93: 276-282.

[33] Javaid A, Bajwa R, Shafique U, et al. Removal of heavy metals by adsorption on Pleurotus ostreatus[J]. Biomass & Bioenergy, 2011, 35: 1675-1682.

[34] Mondal S. Methods of dye removal from dye house effluent-An overview[J]. Environmental Engineering Science, 2008, 25: 383-396.

[35] Salleh M A M, Mahmoud D K, Karim W A W A, et al. Cationic and anionic dye adsorption by agricultural solid wastes: A comprehensive review[J]. Desalination, 2011, 280: 1-13.

[36] Alizadeh R, Kazemi R K, Rezaei M R, et al. Ultrafast removal of heavy metals by tin oxide nanowires as new adsorbents in solid-phase extraction technique[J]. International Journal of Environmental Science and Technology, 2018, 15: 1641-1648.

[37] Hu H, Srinivasan P. Mesoporous high-surface-area activated carbon[J]. Microporous and Mesoporous Materials, 2001, 43: 267-275.

[38] Natarajan S, Bajaj C, Tayade J, et al. Recent advances based on the synergetic effect of adsorption for removal of dyes from waste water using photocatalytic process[J]. Environmental Sciences, 2017, 53: 73-74.

[39] Gondal A, Chang X, Ali M, et al. Adsorption and degradation performance of Rhodamine B over BiOBr under monochromatic 532 nm pulsed laser exposure[J]. Applied Catalysis A: General, 2011, 397: 192-200.

[40] Noman E, Al-Gheethi A, Talip B, et al. Decolourization of Dye Wastewater by A Malaysian isolate of Aspergillus iizukae 605EAN Strain: A Biokinetic, Mechanism and Microstructure Study[J]. Environmental Analytical Chemistry, 2021, 101: 1592-1615.

[41] Ali H. Biodegradation of Synthetic Dyes-A Review[J]. Water, Air, & Soil Pollution, 2010, 213: 251-273.

[42] Forgacs E, Cserháti T, Oros G, et al. Removal of synthetic dyes from wastewaters: a review[J]. Environment International, 2004, 37: 953-971.

[43] Legerská B, Chmelová, D, Ondrejovič M, et al. Degradation of synthetic dyes by laccases-a mini-review[J]. Nova Biotechnol. Chim, 2016, 15: 90-106.

[44] Siddiqui S, Fatima B, Tara N, et al. Recent advances in remediation of synthetic dyes from wastewaters using sustainable and low-cost adsorbents[J]. The Impact and Prospects of Green Chemistry for Textile Technology, 2019, 76: 471-507.

[45] Cheng Z-L, Li Y-X, Liu Z, et al. Study on adsorption of rhodamine B onto Beta zeolites by tuning SiO_2/Al_2O_3 ratio[J]. Ecotoxicology and Environmental Safety, 2018, 148: 585-592.

[46] Al-Gheethi A, Azhar M, Kumar S, et al. Sustainable approaches for removing Rhodamine B dye using agricultural waste adsorbents: A review[J]. Chemosphere, 2022, 287: 254-280.

[47] Liu K, Li H, Wang Y, et al. Adsorption and removal of rhodamine B from aqueous solution by tannic acid functionalized graphene[J]. Colloids and Surfaces A: Physicochemical and Engineering Aspects, 2015, 477: 35-41.

[48] Selvam P, Preethi S, Basakaralingam P, et al. Removal of rhodamine B from aqueous solution by adsorption onto sodium montmorillonite[J]. Hazardous Materials, 2008, 155: 39-44.

[49] Islam A, Ali I, Karim A, et al. Removal of dye from polluted water using novel nano manganese oxide-based materials[J]. Water Process Engineering, 2019, 223: 263-276.

[50] Kant R. Textile dyeing industry an environmental hazard[J]. Nat Sci 4, 2012, 1: 22–26.

[51] Morshed A, Rahman M. A review on the physico-chemical studies of dyeing progress and dyeing kinetics using natural dyes[J]. IOSR Journal of Polymer and Textile Engineering, 2015, 32: 71-75.

[52] Zhu H, Jiang R, Zeng M, et al. Preparation, characterization and dye adsorption properties of γ-Fe_2O_3/SiO_2/chitosan composite[J]. Applied Surface Science, 2011, 2584: 1337-1344.

[53] Christie R. Environmental aspects of textile dyeing[J]. Elsevier, 2007, 64: 35-38.

[54] Nabil G, El-Mallah N, Mahmoud E, et al. Enhanced decolorization of reactive black 5 dye by active carbon sorbent-immobilized-cationic surfactant (AC-CS) [J]. Industrial and Engineering Chemistry, 2014, 20: 994-1002.

[55] Uestuen G E, Solmaz S K A, Birguel A, et al. Regeneration of industrial district wastewater using a combination of Fenton process and ion exchange-A case study[J]. Resources, Conservation & Recycling, 2007, 52: 425-440.

[56] Mittal A, Jhare D, Mittal J, et al. Adsorption of hazardous dye Eosin Yellow from aqueous solution onto waste material De-Oiled Soya: Isotherm, kinetics and bulk removal[J]. Molecular Liquids, 2013, 179: 133-140.

[57] Duran A, Tuzen M, Soylak M, et al. Preconcentration of some trace elements via using multiwalled carbon nanotubes as solid phase extraction adsorbent[J]. Hazardous Materials, 2009, 169: 466-471.

[58] Verma A, Dash R, Bhunia P, et al. A review on chemical coagulation/flocculation technologies for removal of colour from textile wastewaters[J]. Environmental Management, 2012, 93: 154-168.

[59] Patel H. Fixed-bed column adsorption study: a comprehensive review[J]. Applied Water Science, 2019, 96: 245-276.

[60] Leal A, de Lima A, Cruz F, et al. Removal of Remazol Black B dye using bacterial cellulose as an adsorbent[J]. Scientia Plena, 2021, 173: 86-97.

[61] Hu X, Ying G, Chen X, et al. Fourier transform infrared spectroscopy as a novel approach to providing effect based endpoints in duckweed toxicity testing[J]. Environmental Toxicology and Chemistry, 2017,6(2): 346-353

[62] Heravi M M, Zakeri M. Use of Sodium Molybdate Dihydrate as an Efficient Heterogeneous Catalyst for the Synthesis of Benzopyranopyrimidine Derivatives[J]. Synthesis and Reactivity in Inorganic, Metal-organic, and Nano-metal Chemistry, 2013, 43: 211-216.

[63] Pignon J, Lieber S. What relation exists between ethanol, atherosclerosis and high density lipoproteins[J]. Presse Medicale, 1987, 16: 2099-2100.

[64] Smekal W, Werner S, Powell J, et al. Simulation of electron spectra for surface analysis (SESSA): a novel software tool for quantitative Auger-electron spectroscopy and X-ray photoelectron spectroscopy. Surface and Interface Analysis: An International Journal devoted to the development and application of techniques for the analysis of surfaces[J]. Interfaces and Thin Films,2005, 3711: 1059-1067.

[65] Zhou W, Apkarian R, Wang Z, et al. Fundamentals of scanning electron microscopy (SEM)[J]. In Scanning Microscopy for Nanotechnology, 2006, 53: 1-40.

[66] Naderi M. Surface area: brunauer-emmett-teller (BET). In Progress in Filtration and Separation[J]. Academic Press, 2015, 542: 585-608.

[67] Burns R. Mineralogical applications of crystal field theory[J]. Cambridge University Press, 1993, 43: 54-58.

[68] Picollo M, Aceto M, Vitorino T, et al. UV-Vis spectroscopy[J]. Physical Sciences Reviews, 2019, 44: 67-69.

[69] Bacci M, Picollo M, Trumpy G, et al. Non-invasive identification of white pigments on 20th-century oil paintings by using fiber optic reflectance spectroscopy[J]. American Institute for Conservation, 2007, 461: 27-37.

[70] Sykowski P. Ethylene glycol toxicity[J]. American Journal of Ophthalmology. 1951, 34: 1599-1600.

[71] Christensen A, Chevallier M, Skibsted J, et al. Synthesis and characterization of basic bismuth(III) nitrates[J]. Chemical Society-Dalton Transactions, 2000: 265-270.

[72] Gattow G, Schott D. Über Wismutnitrate. III. Zur Hydrolyse von salpetersauren Bi^{3+} Lösungen. Zeitschrift Für Anorganische Und Allgemeine, 1963, 324(12): 31-47.

[73] Alexander M, Bhat P, Samant D, et al. Bismuth(III) nitrate pentahydrate-a mild and inexpensive reagent for synthesis of coumarins under mild conditions[J]. Tetrahedron Letters, 2005, 46: 6957-6959.

[74] Bothwell J, Krabbe S, Mohan R, et al. Applications of bismuth (III) compounds in organic synthesis[J]. Chemical Society Reviews, 2011, 409: 4649-4707.

[75] Al-Gheethi A A, Azhar Q M, Kumar P S, et al. Sustainable approaches for removing Rhodamine B dye using agricultural waste adsorbents: A review[J]. Chemosphere, 2022, 287: 254-268.

[76] Üner O, Geçgel Ü, Kolancilar H, et al. Adsorptive removal of rhodamine B with activated carbon obtained from okra wastes[J]. Chemical Engineering Communications, 2017, 204: 772-783.

[77] Jinendra U, Bilehal D, Nagabhushana B M, et al. Adsorptive removal of Rhodamine B dye from aqueous solution by using graphene-based nickel nanocomposite[J]. Heliyon, 2021, 75: 435-484.

[78] Bhat A, Rashid N, Rather A, et al. Highly efficient catalytic reductive degradation of Rhodamine-B over Palladium-reduced graphene oxide nanocomposite[J]. Chemical Physics Letters, 2020, 243: 754-760.

[79] Heravi M, Zakeri M. Use of Sodium Molybdate Dihydrate as an Efficient Heterogeneous Catalyst for the Synthesis of Benzopyranopyrimidine Derivatives[J]. Synthesis and Reactivity in Inorganic, Metal-organic, and Nano-metal Chemistry, 2013, 43: 211-216.

[80] Lieber C, Leonore M, Michael F, et al. Experimental methods of ethanol administration[J]. Hepatology, 1989, 104: 501-510.

[81] Costa R, Carvalhal A, Bernardes E, et al. Use of potassium iodide in dermatology: updates on an old drug[J]. Anais Brasileiros De Dermatologia, 2013, 88: 396-402.

[82] Hassan I, Keen A. Potassium iodide in dermatology[J]. Indian Journal of Dermatology, Venereology and Leprology, 2012, 78: 390-392.

[83] Roonasi P, Holmgren A. A Fourier transform infrared (FTIR) and thermogravimetric analysis (TGA) study of oleate adsorbed on magnetite nano-particle surface[J]. Applied Surface Science, 2009, 255: 5891-5895.

[84] Jamsheer A F, Kupwade-Patil K, Buyukozturk O, et al. Analysis of engineered cement paste using silica nanoparticles and metakaolin using Si-29 NMR, water adsorption and synchrotron X-ray Diffraction [J]. Construction and Building Materials, 2018, 180: 698-709.

[85] M Wang M, Han J, Guo P, et al. Hydrothermal synthesis of B-doped Bi_2MoO_6 and its high photocatalytic performance for the degradation of Rhodamine B[J]. Physics and Chemistry of Solids, 2018, 113: 86-93.

[86] Dogan U, Dogan M, Onal M, et al. Baseline studies of The Clay Minerals Society source clays: Specific surface area by the Brunauer Emmett Teller (BET) method[J]. Clay Minerals, 2006, 54: 62-66.

[87] Ferrari L, Kaufmann J, Winnefeld F, et al. Interaction of cement model systems with superplasticizers investigated by atomic force microscopy, zeta potential, and adsorption measurements[J]. Colloid and Interface Science, 2010, 347: 15-24.

[88] Dumrongrojthanath P, Phuruangrat A, Thongtem S, et al. Hydrothermal synthesis and characterization of visible light-driven I-doped Bi_2MoO_6 photocatalyst[J]. Iranian Chemical Society, 2019, 16: 733-739.

[89] Liu Z, Liu X, Yu C, et al. Fabrication and characterization of I doped Bi_2MoO_6 microspheres with distinct performance for removing antibiotics and Cr(VI) under visible light illumination[J]. Separation and Purification Technology, 2020, 84: 247-253.

[90] Xia S, Jia R, Feng F, et al. Effect of solids retention time on antibiotics removal performance and microbial communities in an A/O-MBR process[J]. Bioresource Technology, 2012, 106: 36-43.

[91] Yang Z, Wang R, Xu L, et al. Highly efficient flower-like Dy^{3+}-doped Bi_2MoO_6 photocatalyst under simulated sunlight: design, fabrication and characterization[J]. Optical Materials, 2021, 116: 111-114.

[92] Sin J C, Lam S M, Zeng H, et al. Magnetic $NiFe_2O_4$ nanoparticles decorated on N-doped BiOBr nanosheets for expeditious visible light photocatalytic phenol degradation and hexavalent chromium reduction via a Z-scheme heterojunction mechanism[J]. Applied Surface Science, 2021, 87: 559-562.

[93] Phuruangrat, A., Ekthammathat, N., Kuntalue, B., et al. Hydrothermal synthesis, characterization, and optical properties of Ce Doped Bi_2MoO_6 nanoplates[J]. Journal of Nanomaterials, 2014, 934165.

[94] Ferrari, L., Kaufmann, J., Winnefeld, F., et al. Interaction of cement model systems with superplasticizers investigated by atomic force microscopy, zeta potential, and adsorption measurements[J]. Journal of Colloid and Interface Science, 2010, 347(1): 15-24.

[95] Dumrongrojthanath P, Phuruangrat A, Thongtem S, et al. Hydrothermal synthesis and characterization of visible light-driven I-doped Bi_2MoO_6 photocatalyst[J]. Iranian Chemical Society, 2019, 16: 733-739.

[96] Liu Z, Liu X, Yu C, et al. Fabrication and characterization of I doped Bi_2MoO_6 microspheres with distinct performance for removing antibiotics and Cr(VI) under visible light illumination[J]. Separation and Purification Technology, 2020, 84: 247-293.

[97] Tang Y, Lin T, Jiang C, et al. Renewable adsorbents from carboxylate-modified agro-forestry residues for efficient removal of methylene blue dye[J]. Physics and Chemistry of Solids, 2021, 121: 149-151.

[98] Xiao X, Wang Y, Cui B, et al. Preparation of MoS_2 nanoflowers with rich active sites as an efficient adsorbent for aqueous organic dyes[J]. New Journal of Chemistry, 2020, 411: 4558-4567.

[99] Jiang L, Wen Y, Zhu Z, et al. A Double cross-linked strategy to construct graphene aerogels with highly efficient methylene blue adsorption performance[J]. Chemosphere, 2021, 265: 129-169.

[100] Kinniburgh D G. General purpose adsorption isotherms[J]. Environmental science & technology, 1986, 20: 895-904.

[101] Abollino O, Aceto M, Malandrino M, et al. Adsorption of heavy metals on Na-montmorillonite. Effect of pH and organic substances[J]. Water Research, 2003, 37: 1619-1627.